Fall 2007

Brain segmentation using endogenous contrast mechanism using breath holding fMRI signal for tissue characterization

Samata Mukesh Kakkad
New Jersey Institute of Technology

Copyright Warning & Restrictions

The copyright law of the United States (Title 17, United States Code) governs the making of photocopies or other reproductions of copyrighted material.

Under certain conditions specified in the law, libraries and archives are authorized to furnish a photocopy or other reproduction. One of these specified conditions is that the photocopy or reproduction is not to be "used for any purpose other than private study, scholarship, or research." If a, user makes a request for, or later uses, a photocopy or reproduction for purposes in excess of "fair use" that user may be liable for copyright infringement,

This institution reserves the right to refuse to accept a copying order if, in its judgment, fulfillment of the order would involve violation of copyright law.

Please Note: The author retains the copyright while the New Jersey Institute of Technology reserves the right to distribute this thesis or dissertation

Printing note: If you do not wish to print this page, then select "Pages from: first page # to: last page #" on the print dialog screen

ABSTRACT

BRAIN SEGMENTATION USING ENDOGENOUS CONTRAST MECHANISM USING BREATH HOLDING FMRI SIGNAL FOR TISSUE CHARACTERIZATION

by

Samata Mukesh Kakkad

MRI has fast become the modality of choice for the analysis of the complexity of the human brain. MRI is a non-invasive method and gives high spatial resolution maps of the brain with soft tissue contrast. Conventional MRI technique modified to be used to image the functionality at high temporal resolution is known as fMRI. In fMRI the BOLD signal we measure is the hemodynamic response to neuronal and vascular changes at rest or in response to a stimulus where the various tissue types will have a different response.

While fMRI has been traditionally been used to detect and identify eloquent regions of the cortex corresponding to specific tasks/stimulus, a number of groups have also used fMRI to study cerebrovascular changes and its consequence on the BOLD signal. A number of different perturbation methods including breath holding, hypercapnia, inhalation of various gas mixtures, and injection of acetozolamyde has been used to study spatio-temporal changes in the fMRI signal intensity. Spatiotemporal changes corresponding to changes in cerebral blood flow (CBF), cerebral blood volume (CBV), oxygen extraction fraction (OEF), and other physiological factors are then estimated and differences between diseased regions and healthy regions are then elucidated.

BRAIN SEGMENTATION USING ENDOGENOUS CONTRAST MECHANISM USING BREATH HOLDING FMRI SIGNAL FOR TISSUE CHARACTERIZATION

by
Samata Mukesh Kakkad

A Thesis
Submitted to the Faculty of
New Jersey Institute of Technology
in Partial Fulfillment of the Requirements for the Degree of
Master of Science in Biomedical Engineering

Department of Biomedical Engineering

January 2008

APPROVAL PAGE

Brain Segmentation Using Endogenous Contrast Mechanism Using Breath Holding fMRI Signal for Tissue Characterization

Samata Mukesh Kakkad

Dr. Sergei Adamovich, Co-Advisor — Date
Assistant Professor of Biomedical Engineering, NJIT

Dr. Tara L. Alvarez, Co-Advisor — Date
Associate Professor of Biomedical Engineering, NJIT

Dr. Bharat B. Biswal, Committee Member — Date
Associate Professor of Department of Radiology, UMDNJ

BIOGRAPHICAL SKETCH

Author: Samata Mukesh Kakkad

Degree: Master of Science

Date: January 2008

Undergraduate and Graduate Education:

- Master of Science in Biomedical Engineering,
  New Jersey Institute of Technology, Newark, NJ, 2008

- Bachelor of Science in Biomedical Engineering,
  D. J. Sanghvi College of Engineering, Mumbai, India, 2006

Major: Biomedical Engineering

'If we knew what it was we were doing, it would not be called **research**, would it?'

- Albert Einstein

ACKNOWLEDGMENT

Firstly, I would like to thank Dr. Sergei Adamovich, my advisor at New Jersey Institute of Technology for supporting my work at UMDNJ. Dr. Sergei has always helped me without any hesitance whenever I approached him. I would like to thank Dr. Alvarez for her support and encouragement. I derive my inspiration and dedication towards my research work from her.

I express my greatest gratitude to Dr. Bharat Biswal, my research supervisor. He provided me with this research opportunity and made available the resources for it. Dr. Biswal has always been encouraging and supporting and has guided me at every step. I would like to mention Dr. Shridhar Kannurpatti here and thank him for helping me with research problems as they arose. I also thank Nirvish Shah, PhD student at 3T lab for all his help. My best wishes to my fellow graduate students Sheela Nagraj, Parina Ghandhi, Priyanka Shah and Don Adams; working with all of you was a pleasure and a memorable one.

Lastly, I thank my parents and my grandparents for all their support and all my friends who have tolerated me through all my tantrums.

TABLE OF CONTENTS

TABLE OF CONTENTS
(CONTINUED)

Chapter **Page**

LIST OF TABLES

LIST OF FIGURES

LIST OF FIGURES
(Continued)

Figure **Page**

CHAPTER 1

INTRODUCTION

1.1 Background Information

MRI has become the modality of choice for the analysis of the complexity of the human brain. It is a non-invasive method and gives high resolution spatial maps of the brain with soft tissue contrast [1-4]. Conventional MRI technique modified to be used to image the functionality at high temporal resolution is known as functional magnetic resonance imaging (fMRI) [5-8]. In fMRI, the BOLD signal we measure is the hemodynamic response to neuronal and vascular changes (at rest or) in response to a stimulus where various tissues have a varying response [9].

In addition to providing high resolution images with superior contrast between gray matter, white matter, and CSF, MRI images can be obtained using a number of different contrasts using T1, T2, proton density, and chemical shift imaging [10-11]. As a consequence, imaging parameters can be optimized to obtain images with certain weightings to highlight specific contrasts in specific tissue types. A number of different image processing algorithms including edge detection, boundary tracing, voxel based thresholding, seed growing, and template models [12-15] are then applied to the MR image. Processed image(s) obtained are then segmented using supervised, semi-automated, or automated methods to determine the regions of interest [16-18].

For a number of applications, however, the choice of finding imaging parameters that will give optimal signal-to-noise ratio (SNR) and contrast-to-noise ratio (CNR) are not straight forward and depend on a number of parameters including field strength, the pulse sequence being used, the organ being imaged. As a result, several groups have used

an alternative strategy whereby instead of a single image with the desired contrast, a set or a series of images are obtained each with different weightings [19-20]. These images are then used together to decompose them into a set of images each with a specific contrast (T1 vs T2 vs PD) and consequently segment the images with better demarcation between the regions of interest than obtained using a single image [21]. Such methods have been used to segment ischemic regions after a stroke, from other gray matter and white matter regions [22-24].

Rosen et al [25] first introduced the use of contrast agents to study cerebral perfusion. The technique known as dynamic susceptibility contrast (DSC-MRI) involves the injection of a bolus of MR contrast agent (typically 0.1 to 0.3 mmol/kg body weight), which causes spin dephasing (i.e., decrease in T_2 and T_2*) during its fast passage through the tissue [26] which is measured as a loss in the MRI signal. This provides an enhanced T1 contrast with additional information about different physiological parameters related to cerebral blood flow (CBF), cerebral blood volume (CBV) and the mean transit time (MTT) of blood through the voxel. The contrast agent produces a significant drop in the MR signal resulting in compartmentalization even though the vascular space is a small fraction of the total tissue volume (~5% in the human brain). This effect due to susceptibility extends beyond the vascular space [26-27] and dominates over the T_1 relaxation enhancement. In regions where the blood brain barrier has been compromised, the contrast agent escapes from the intravascular space resulting in a decrease in the susceptibility effects, resulting in an increase in the MR signal. Since the transit time of the bolus is only a few seconds (and even shorter in animal models), high temporal resolution is required to sequentially obtain images before, during, and after the contrast

injection. The practicability of DSC-MRI has greatly increased with improvement in hardware and software development that has enabled the widespread availability of fast acquisition pulse sequences including echo planar imaging (EPI).

Perfusion and other physiologically relevant parameters have been used extensively to segment different tissue types and to differentiate healthy from diseased tissues (25). Dynamic susceptibility imaging using T1-weighted contrast has typically been used to characterize and quantify various physiological parameters including blood flow, transit time, time to peak, etc (30, 31). These methods have been used extensively in a number of clinical populations including tumor (32) and stroke (33).

Recently, Kao et al (34) used independent component analysis (ICA), thresholding, and Bayesian estimation to concurrently segment different tissues, i.e., artery, gray matter, white matter, vein and sinus, choroid plexus, and cerebral spinal fluid, with corresponding signal-time curves on perfusion images of five normal volunteers. Spatiotemporal hemodynamics, sequential passage and microcirculation of contrast-agent particles in these tissues were decomposed and analyzed.

Considerable effort has been directed towards optimizing the detection of MR signal changes following sensory, motor, and cognitive stimulus paradigms [5-8]. Under optimal conditions, the task-induced (or activation) signal increases by 5-10% above the mean baseline (or resting) signal intensity [35]. Most fMRI studies are conducted using T2*-weighted pulse sequences that are sensitive to blood oxygenation level dependent (BOLD) signal changes. The premise of the BOLD fMRI paradigm is that the neuronal activation leads to vasodilation, with a concomitant increase in CBF, CBV and oxygen delivery. Since the relative CBF changes exceed the CBV changes, and the

accompanying oxygen extraction changes only by a small amount, the total amount of paramagnetic deoxyhemoglobin in the blood decreases with activation. This increase in the net difference between the oxyhemoglobin and deoxyhemoglobin concentrations in the blood reduces the tissue-blood susceptibility difference, which leads to less intravoxel dephasing, resulting in an increase in the T2*-weighted MR signal intensity [8]. This increase in the T2*-weighted signal during neuronal activation has been modeled as an increase in neuronal activity convolved with the intrinsic hemodynamic response [36-37]. Consequently, variations in the temporal characteristics of the MR signal may be attributable either to differences in the neuronal activity or to the intrinsic hemodynamic response. The conventional approach in fMRI studies has been to present a subject with a task and then look for activation-induced changes (typically 5-10%) in the MR signal, relative to a resting state. Typically in fMRI protocols, blocks of images obtained during rest are alternated with blocks of images obtained during the stimulus condition. This paradigm is repeated several times so that a robust response might be computed.

While fMRI has been traditionally been used to detect and identify eloquent regions of the cortex corresponding to specific tasks/stimulus, a number of groups have also used fMRI to study cerebrovascular changes and its consequence on the BOLD signal. A number of different perturbation methods including breath holding (38-42), hypercapnia (43-44), inhalation of various gas mixtures, and injection of acetazolamide (45) have been used to study spatio-temporal changes in the fMRI signal intensity. Spatiotemporal changes corresponding to changes in CBF, CBV, OEF, and other physiological factors are then estimated and differences between diseased regions and healthy regions are then elucidated (46-48).

The increase in task induced signal intensity is determined by the increase in neural activity convolved with the intrinsic vascular sensitivity. Thus, the signal intensity in a voxel can increase either due to an increase in neuronal activity or intrinsic vascular sensitivity. Correlation methods that are commonly used in fMRI studies detect absolute signal changes between control and activation conditions. Thus, if two different voxels that, during rest, have signal intensities of, say, 100 and 1000 change to 150 and 1050 during task activation (assuming the same noise levels), they would have the same correlation with expected signal change. While calculating the percent signal-change compared to the resting-state baseline condition might overcome the problem of correlation, it still cannot quantify and separate the effects of neural activation from those of intrinsic vascular sensitivity. To differentiate between neuronal activities versus intrinsic vascular effects, a number of groups have used moderate hypercapnic response in addition to task induced signal changes to quantify signal changes [43 44]. Recently, it has been shown that moderate respiratory hypercapnia by breathing a gas mixture (5% CO2, 20% O2 and 75% N2) is similar to breath-holding and subsequently employed breath holding to scale task induced signal changes in fMRI data sets [49]. In the study, the absolute change of task activation was divided by the absolute change with hypercapnic signal change during breath holding to obtain a hemodynamically scaled activation response on a voxel-by-voxel basis.

1.2 Objective

The aim of this study was to use physiological perturbation methods like breath holding in conjunction with gamma-variate fit parameters to estimate various physiological relevant parameters and then use these parameters to differentiate between various tissue types including gray matter, white matter, and large vessels. A comparison between the segmentation of gray matter, and white matter using two different methods i.e., gamma-variate parameters obtained from the breath holding studies and the high resolution anatomy demonstrated a significant overlap between the two methods.

1.3 Outline of the project

This Thesis is organized as follows: Chapter 2 describes MRI based tissue segmentation. In this chapter different methods and procedures implemented in segmentation are discussed. The following chapter, Chapter 3 describes dynamic imaging and how it is used for tissue segmentation is described. Various pre-processing strategies involved in fMRI are included. Chapter 4 explains the experimental paradigm used in this study along with the imaging methods and the data analysis methods. Chapter 5 holds the results of the project. The last chapter, Chapter 6 is the concluding chapter which discusses the advantages and disadvantages of the proposed study. Future experiments that can be done to improve the efficacy of the study have also been described.

CHAPTER 2

MRI BASED SEGMENTATION

2.1 Magnetic Resonance Imaging

The principle behind Magnetic Resonance Imaging (MRI) is placing protons in a magnetic field and examining their behavior by varying the magnetic fields. Protons have two kinds of motions. Motion in an orbit around the nucleus is called orbital rotation. The proton also spins about an axis, this motion is called spinning. The rotational motion of a body is described by its Angular momentum. Both orbital and spinning of the proton have different angular momentums associated with them. The atom always tries to attain a stable state by the arranging its protons in anti-parallel state (spin up and spin down); that is their angular momentums are in the opposite directions. This is called spin pairing. Therefore, the resultant angular momentum of the nucleus would be the total spin of the unpaired neutron and proton and their orbital momentum.

The motions of protons also have an associated Magnetic Dipole Moment (MDM). MDM of the protons of an element indicates how fast they align themselves along an external magnetic field. It is this characteristic of the element that is detectable in MRI.

When the protons are placed in an external magnetic field their axes which were initially randomly oriented align themselves at an angle with respect to the magnetic field. Due to this orientation they spin about the magnetic field see figure 2.1, this spinning is called precession.

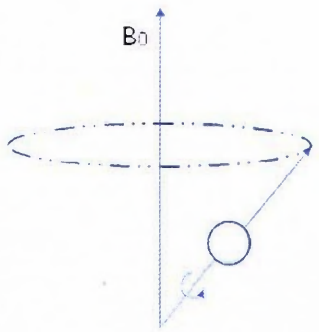

Figure 2.1 A spinning Nucleus precessing about B_0, B_0 is the strength of the applied magnetic field

The frequency of precession is called the Larmor frequency which is given by

$$V_L = \gamma H / 2*pi \quad (1)$$

Where V_L is Larmor frequency, γ=gyromagnetic ratio, H=magnetic field.

Gyromagnetic ratio is the ratio of the MDM and the spin angular momentum;

$$\gamma = \mu / I*\hbar \quad (2)$$

Where γ is the gyromagnetic ratio, μ is MDM, $I*\hbar$ is spin angular momentum I is nuclear spin, $\hbar$ is planks constant *2*pi.

The gyromagnetic ratio shows that there is a unique value of Larmor frequency for different nuclei. The magnetic induction and the gyromagnetic ratio produce the Larmor frequency of precession. This forms the basis of medical imaging of the protons. Since we have a unique Larmor frequency for different nuclei this process is able to distinguish between different nuclei. Also a same nucleus will have a different Larmor frequency when placed in different external magnetic fields. MR imaging is done using hydrogen protons as 80% of the human body contains water. Varying the Larmor frequency for the imaging proton gives the ability to recognize the nucleus in 3D space. This gives a different signal from the gray matter, white matter, cerebral spinal fluid (CSF) acquiring high resolution anatomical map.

Contrast characteristics in images are obtained by imaging parameters like T1, T2, proton density and chemical shift of the protons, according to the application. Image processing on these MR images is done to emphasize on the desired characteristic. Segmentation now performed on the processed images will group separately regions having the same characteristics. A single contrast image or multiple contrast images can be used to improve on the segmentation of the regions.

2.2 Segmentation

Preprocessing before segmentation is very important and the noise that's present can influence the segmentation results significantly. After performing various preprocessing procedures feature extraction is done. Feature extraction involves selecting only a certain characteristics from the image dataset. Instead of performing segmentation on the dataset as a whole, segmentation is done on a feature or more depending on the application. Image features can be simply the pixel intensity or some calculated feature like edge pattern or blood flow. Feature selection will decide the success rate of the segmentation. It plays an important role when dimensionality is of computational weigh down.

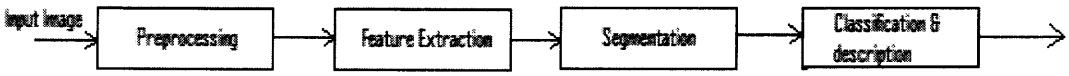

Figure 2.2 A schematic for segmentation procedure.

2.2.1 Feature Selection

Segmentation is applied on the basis of feature selection which provides the feature vector that is used for grouping.

Pixel intensity-based feature: Here the input is pixel intensity which is the gray scale value from either a single image, volume of dataset or a multispectral dataset. Multispectral dataset is collected from multi-echo image acquisition or multi-sequence image acquisition. The additional dataset are simply added together to form an N dimensional feature vector.

Calculated pixel intensity-based feature: This feature is sensitive to noise and does not provide a stable segmentation results. Therefore, this feature extraction is implemented only of an operator defined region. Advantage of this feature extraction is that it is less sensitive to image non-uniformity. Calculated pixel-intensity has increased with the advances in Dynamic imaging. Parameters calculated are cerebral blood flow, blood volume, oxygenation or metrics relating to flow of contrast material.

Edges and texture-based feature: The non-uniform nature of MR images makes it unreliable to use a global threshold; an additional feature is needed for stable segmentation. Edge detection method has been implemented using either the Marr-Hildreth operator [54] or the Canny edge detector [55]. Edge detection method [56] has not proven to have shown reliable results. Texture based feature selection has been used but for classification and not to demarcation of regions. Moreover for texture-based features is applied using a large dataset or an alternate statistical texture feature where pixel intensity from the 8 neighbor is considered. No reports on the quality of segmentation using this method have been reported. Texture feature can be applied and after performing discrimination analysis the most relevant feature can be selected or to label smaller region as region of interest.

In this project calculated pixel-based feature is used for brain tissue segmentation. The parameters used here include from the calculation by gamma variate to fit the fMRI response to breathe holding paradigm like time to initiate response (t_0), time to maximum signal intensity (T_{max}), signal area under the curve (S_{area}), etc.

2.2.2 Segmentation

Segmentation is essentially divided into which include the signal gray scale image segmentation which uses a single 2D or 3D image and the multispectral image segmentation which uses multiple MR images with different gray scale contrasts. These two groups are further divided as shown in the figure 2.4.

Gray Scale Single Image Segmentation: A single image is used for the segmentation procedure. Following are the types of single image segmentation-

- Thresholding-based segmentation method. A global threshold is applied on the dataset to distinguish between two regions. The problem with this method is to find the ideal threshold value, which makes this method subjective. One way of selecting the threshold is by plotting the histogram of the image. As seen in Figure 2.3 the histogram shows two distinct frequency peaks called bimodal distribution. A threshold value could now easily be selected to demarcate out one region from the other.

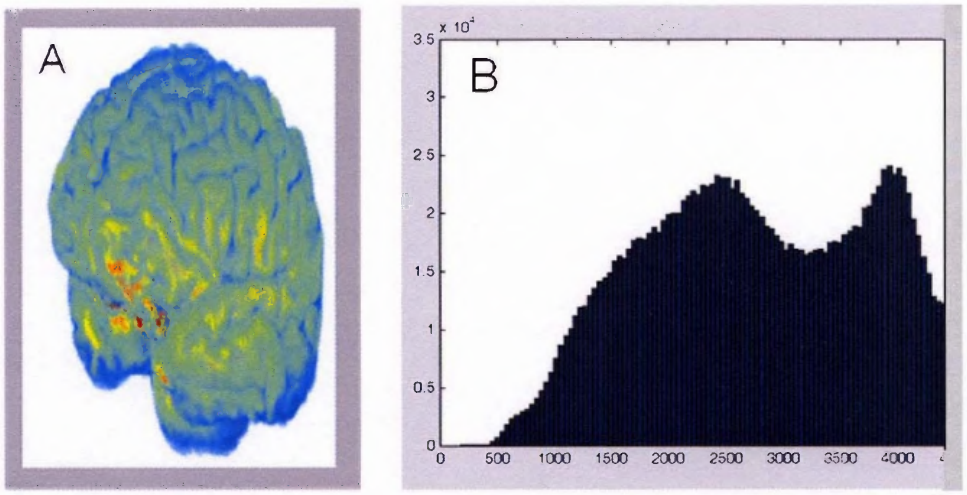

Figure 2.3 A- Brain map using MRI; B-histogram of the brain map.

The threshold value is calculated from the 'goodness function' with the objective, that the region can be distinguished from its environment. Local threshold could be applied. Thresholding has limited application due to the variability in the MR data and noise.

- Edge-based segmentation method. This detects the high frequency edges to segment between the regions. A pixel is selected and is compared to the neighboring pixels to determine a gradient and trace a boundary. However in presence of noise the pick of the initial pixel is critical. In addition, this method can be only be used to trace boundaries of large region and cannot be used for tissue segmentation.
- Seed growing segmentation. A seed and a threshold are selected by the user. The algorithm grows around the seeds by comparing the seed with the neighboring pixels. If the neighboring pixel is within the threshold then it is included in that region and this pixel then becomes the new seed.

Gray scale single image segmentation has limited application and can be used only for simple structures.

Gray scale single image segmentation has limited application and can be used only for simple structures.

Multi-spectral Image Segmentation: This method of segmentation uses additional images which would hold different unique characteristics of that image. Multi-spectral is further divided into the following-

- Supervised Segmentation Method. Pattern recognition and Algebraic approaches require some kind of operator supervision during the segmentation method and are classified as supervised segmentation (see figure 2.4). Pattern recognition either segments the dataset depending on its pattern by using parametric methods where there is an assumption of certain feature distribution or non-parametric method where k nearest neighbor is rely on actual distribution trained themselves. Algebraic method can deal with partial volume effect and are well suited for images which clearly identified signature vectors. Since the supervised methods have some kind of dependency on the operator there will be inter and intra operator variability.
- Unsupervised Segmentation Method. This technique is also known as 'Clustering'. Clusters are formed automatically containing a feature without the operator's interference in the segmentation method. K-mean and fuzzy c-means are employed for MR image segmentation. ISODATA clustering method is an extension of k-means. Unlike the feature-space database where the features obtained are compared to a table ISODATA automatically detects the number of clusters. In this project ISODATA is used for the brain tissue segmentation on

the breath holding fMRI datasets. The ISODATA segmentation algorithm is explained in the following subsection.

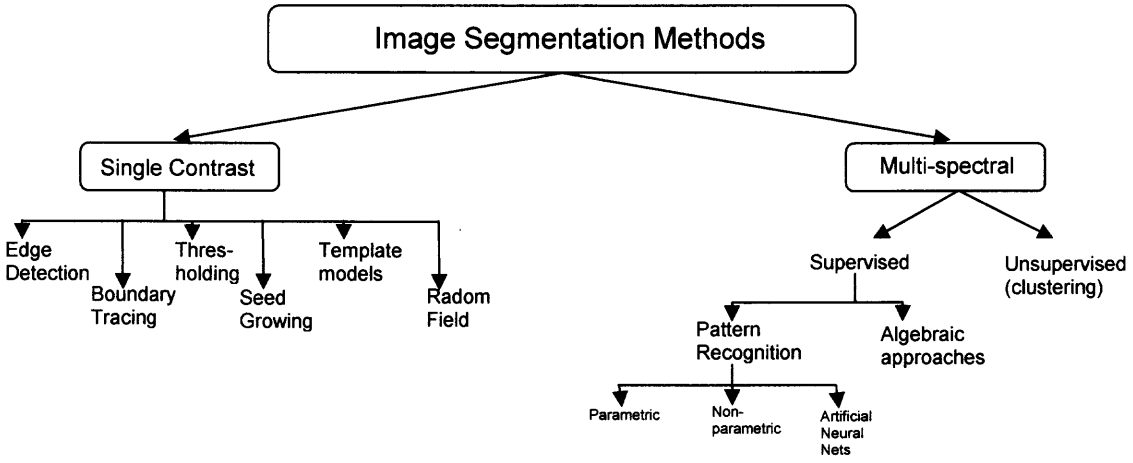

Figure 2.4 Classification Image segmentation methods.

2.2.3 Clustering ISODATA

Clustering is the classification of the dataset into smaller dataset (clusters), in a way that these clusters contain datasets that have common characteristics. An unsupervised classification method, the ISODATA technique was used to segment the gray matter and white matter. ISODATA stands for *Iterative Self-Organizing Data Analysis Techniques*. It follows the K-mean algorithm. The advantage of this technique is that it allows the categorization and selecting the number of clusters. Five to ten clusters are usually chosen; a single voxel does not classify as an individual tissue type. Mean values of clusters are compared thus using a soft thresholding method. Neighboring clusters tissue influence the categorization. Equation for mean squared error (MSE) is shown in equation 3.

$$MSE = \Sigma [x\text{-}c(x)]^2 / (N\text{-}C) \qquad 3$$

Since it is unsupervised segmentation method the algorithm is more sophisticated which allows the number of clusters to be automatically adjusted during the iteration by merging similar clusters and splitting clusters with large standard deviations. The algorithm is initiated by defining various parameters. **K** = number of clusters desired; **I** = maximum number of iterations allowed; **P** = maximum number of pairs of cluster which can be merged; **theta-S** = a threshold value for minimum number of samples in each cluster can have which is used for discarding clusters; **theta-SD** = a threshold value for standard deviation which is used for split operation = a threshold value for pair wise distances which is also used for merge operation.

Steps involved in the algorithm of ISODATA clustering: Initialization is done by selecting N number of the number of cluster that are of interests. The algorithm then selects N random clusters center called centroid. By calculating distance from the centroid and voxels were assigned to a cluster. If the number of voxels in a cluster is less than a predefined threshold then the cluster is discarded. Mean and standard deviation of the cluster is calculated and a new centroid is assigned to each cluster. If the number of clusters is less than number assigned N, then the cluster is split according to the standard deviation and the actual distance. If the number of clusters is more than N, then clusters are merged considering the same factor. Again the mean and standard deviation is calculated and the centroid is reassigned. The whole procedure is repeated till 1 the initialized number of iterations is completed.

CHAPTER 3

DYNAMIC MRI

3.1 Functional Magnetic Resonance Imaging (FMRI)

Oxygenated blood behaves as diamagnetic while deoxygenated blood behave as a paramagnetic as it has four free electrons in the outermost shell. A paramagnet will vary the local magnetic susceptibility to the surrounding, resulting in decrease in the T2 and T2* times. When any kind of neuronal activity takes place there is consumption of the energy and an increase in demand for oxygenated blood. This increase in demand for oxygenated blood is met by the increase in blood flow and blood volume with vasodilation. The decrease in oxygen level in the blood resultant to the neuronal activity is comparatively less to the increased level of oxygen in response to the requirement of oxygenated blood. The net oxygen level in blood is an increase in the oxy-hemoglobin. This reduced the susceptibility gradient that was present between the oxygenated blood and the surrounding tissue in the absence of the neural activity. Whenever a task is performed, the region in the brain responsible for the control of the task will perform some kind of neuronal activity and thus there is an increase in oxygen supply to that region. A stronger MR signal is received from that region, see figure 3.1. This technique of imaging is also called Blood Oxygen Level Dependent (BOLD) imaging.

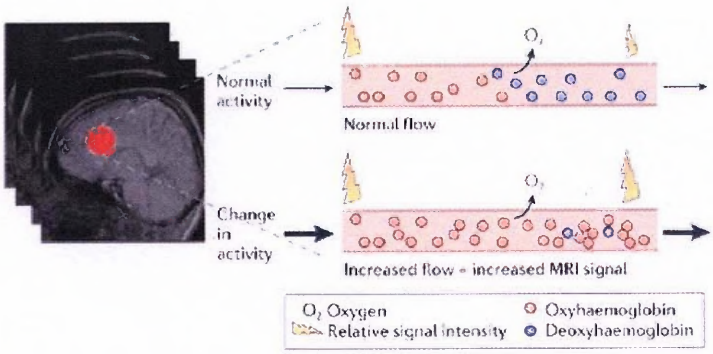

Figure 3.1 An increase in oxyhemoglobin is seen at the region of neural activity. Increased level of MRI signal is acquired from that region.

FMRI was first proposed by Seiji Ogawa in 1990 for the functional mapping of the human brain. It has provided a technique to compare a functional region with high resolution spatial maps.

3.2 Dynamic Susceptibility Contrast (DSC)

Magnetic susceptibility is the ability of matter to vary the external magnetic field to induce a change in the effective magnetic field within and on its surrounding. Injecting a MR contrast agent like Gadolinium (Gd) variation in the magnetic susceptibility of the surrounding structure is achieved to improve the contrast resolution. The introduction of gadolinium changes the local relaxation times of the structure in comparison with the surrounding structures as the contrast agent passes through.

3.3 Indicator Dilution Theory

Circulation function: Blood flow is controlled according to the tissue requirement. Blood flow does not increase throughout the body when there is a high requirement need by a tissue. The local blood vessels play a role by vasodilation or vasoconstriction in accordance to the need of the underlying tissue. Carbon dioxide, oxygen, waste products

and other nutrients control the local activity along with the nervous system. Cardiac output, neuronal and hormonal controls maintain the blood pressure.

Blood flow through a vessel is determined by the pressure gradient present across the blood vessel and the impedance offered by it. Therefore blood flow (Q)

$$Q = \textbf{Del}\ P \backslash R \qquad 4$$

[by ohm's law] blood flow is the amount of blood flowing over a known time duration.

When a contrast agent or dye is injected it is introduced into the circulation system. The concentration of the contrast agent is measured over a period of time in a blood vessel distant from the point of entry. Following a rise in the concentration curve to a peak value, it then falls immediately. In all the cases, the concentration curve rises again by a small amount compared to the first increase and falls again due to recirculation. For calculating the blood flow, the concentration curve is extrapolated to zero after its first peak and the area under the curve is estimated, to obtain the mean concentration of the contrast agent over a known duration. The distribution of the contrast agent characterizes the properties of the vascular vessel in which it flows. The concentration-time curve of the first pass of the contrast agent is then used for the evaluation of various physiological parameters.

Dynamic imaging is done with MRI using MR contrast agent, besides having a high resolution it is a non-invasive method.

3.4 Gamma-Variate

The gamma variate follows a gamma distribution, which is a 2-parametric family of probability distribution function (PDF). It involves a shape factor (r) and a scale factor (b); these factors follow a wide range. The constant Q compensates for the range of the shape and scale factors. Comparing the gamma variate with the indicator dilution theory and the concentration-time curve; for the vasculature, the conductance of the vessel is the scale factor and the distensibility is the shape factor [50].

The development of faster acquisition pulse sequences has allowed imaging of concentration time curves of intravascular bolus injection of a paramagnetic MRI tracer. Various physiological parameters like CBV, CBF are then calculated from these concentration time curves. Once the bolus of a non-diffusible tracer has been introduced into a feeding vessel the particles of the tracer flow in a different path and the distribution of their transit time is characterized by the vascular structure and the blood flow.

Therefore,

$$C_v(t) = C_a(t) * h(t) \qquad 5$$

where h(t) is the probability density function of the transit times, C_a is the arterial input and C_v is the concentration of the tracer at the venous output.

$$MTT = \int h(\tau)d\tau \,/\, \int h(\tau)d\tau; \qquad 6$$

and

$$CBV = \int C_{voi}(\tau)d\tau \,/\, \int Ca(\tau)\, d\tau \qquad 7$$

where MTT is the mean transit time. By central volume theorem we have,

$$MTT = CBV/Ft \qquad 8$$

where Ft is the tissue flow. The fraction of tracer present at time t define the residue function R(t),

$$R(t) = [1 - \int h(\tau)d\tau] \qquad 9$$

Therefore, R(0)=1 and R(t) is positive, decreasing function of time. The concentration within the volume of interest in terms of residue function is given by,

$$C_{voi} = F(t) \int Ca(\tau)\, R(t-\tau)d\tau \qquad 10$$

The central equation states that the initial height of the deconvolved concentration time curve equals the flow, F(t). There are two techniques of deconvolve this equation. 1) Model dependent technique where the residue function is constraint by a defined function. This technique assumes the prior knowledge of the underlying vasculature. Disadvantage of this technique is that it will not predict a good flow if the underlying residue is not uniform. 2) Model independent techniques. Here the residue functions and the tissue flow is determined experimentally. Non-parametric deconvolution can be achieved by transform or the algebraic approach. Since convolution in time domain is multiplication in the frequency domain the residue function can be easily be calculated as,

$$R(t) = Ft^{-1}\, F^{-1} [F\{Cvoi(t)\} / F\{Ca(t)\}] \qquad 11$$

Also the frequency domain separates out the frequency distribution of the data, the noise characterized the high frequency while the physiological parameters comprised of the low frequencies. Since this approach is very sensitive to noise, the noise can be filtered out. The algebraic approach reformulates the convolution integrals into matrices in the form of A.b=c.

Ostergaard et al [30-31] have compared the errors of estimating CBF using parametric and non-parametric deconvolution techniques. They had modified these techniques by using nonparametric singular value decomposition (SVD) to obtain a better estimate of the flow parameters. The proposed method using non-parametric SVD gave comparable flow independent underlying vascular structure. Several other methods have been proposed to get more accurate and reliable perfusion estimates

Breath hold task of fMRI does not involve any kind of neuronal activity and has been used for scaling purpose of the fMRI data.

3.5 Preprocessing

Preprocessing of the MRI data is very important as the percentage signal change during task/stimulus activation is about 3-5%. Physiological noise can easily amount up to 1-2%. However, in the presence of head motion, signal changes due to the movement of head can be more than 10%, in which case the noise could either be mislead to activation or noise could suppress activation. MR is sensitive to the noise factor and it is required to improve the Signal to Noise Ratio (SNR) before performing any kind of analysis on the dataset. The various sources of noise could be from free electron collision resulting in thermal noise, scanner generated drift or gradient field non-uniformity resulting in system noise, noise from head motion and physiological parameters like heat beat, respiration which results in motion and physiological noise.

Preprocessing is mainly done to remove the variability of the signal, to increase the signal to noise ratio and to prepare the dataset for further statistical analysis.

3.5.1 Slice acquisition time correction

In echo planner imaging (EPI) technique of image acquisition an interleaved form of acquisition of data is done to avoid the influence of the neighboring slice since EPI is a fast imaging technique. Therefore here first the odd number slices are collected followed by the acquisition of the even number slices, see figure 3.2. Since interleaved acquisition technique is adopted it misses the actual shape of the hemodynamic response. This error is corrected by using a modified predicted hemodynamic response which is compared to each slice with slightly different timings. The amplitude of the MR response is estimated by interpolation of intensity of the slice in the time domain.

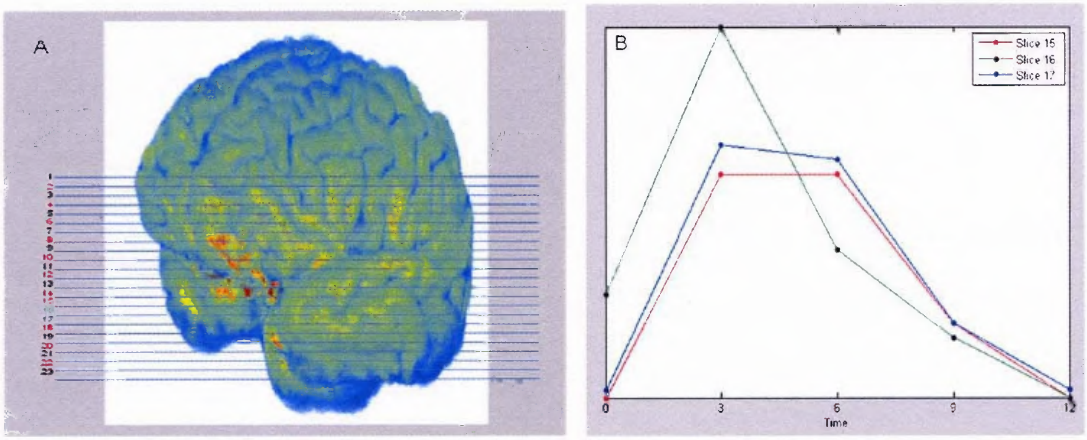

Figure 3.2 A- shows the interleaved acquisition; B-data acquired from slice 15, 16, 17. It can be seen from B that the hemodynamic response shape is missed by the interleaved acquisition.

3.5.2 Head motion correction

The fMRI data acquired represents a unique data from every voxel mapping of the brain. A slight motion in the head of the subject results in the averaging of signal from two or more neighboring voxels. Also if the adjacent voxels have a very different property there will be a large change in signal. Motion error can be minimized by subject compliance, making the subject comfortable in the scanner. Foam padding should be placed to

minimize the involuntary head motion due to certain tasks. Motion correction is applied it follows: the image volume is aligned to a reference volume for co-registration of the dataset. This process is done using rigid body transform where the co-registration is done by translation and rotation is three dimensions. A cost function checks for how well the co-registered images match with each other. A simple cost function would involve calculating the sum of squared intensity differences between the image and the reference. Now spatial interpolation is performed to construct the images as there was no motion using the co-registration parameters. The interpolation can be linear where each interpolated point is the weighted sum of the adjacent points, the other interpolation technique can be a sinc or a spline.

3.5.3 Normalization

Normalization is performed for inter subject comparison for a better understanding of the brain functioning. The functional maps have a very low spatial resolution of the brain are co-registered with the high anatomical maps using rigid body transformation to understand the region of interest. In normalization, co-registration of the brain maps is performed to a standard for the stereotactic space like the Talairach space. It considers the overall size of the brain and also the anatomical feature. Normalization allows inter subject and inter study comparison.

3.5.4 Spatial and Temporal smoothing

FMRI data has noise added due to physiological parameters like heart beat and respiration. Since we know the frequency of these physiological parameters they can be

filtered out. Also the high frequency spatial component which results in the blurring of the image is filtered out normally using a Gaussian filter.

3.6 Data Analysis

Data analysis is the examination of the data and summarizing data to extract important information. For fMRI data analysis various methodologies are adopted. Without much prior information activation due to the task performed can be identified by correlation method and thresholding. Figure 3.3 shows a schematic diagram of fMRI functioning and data processing.

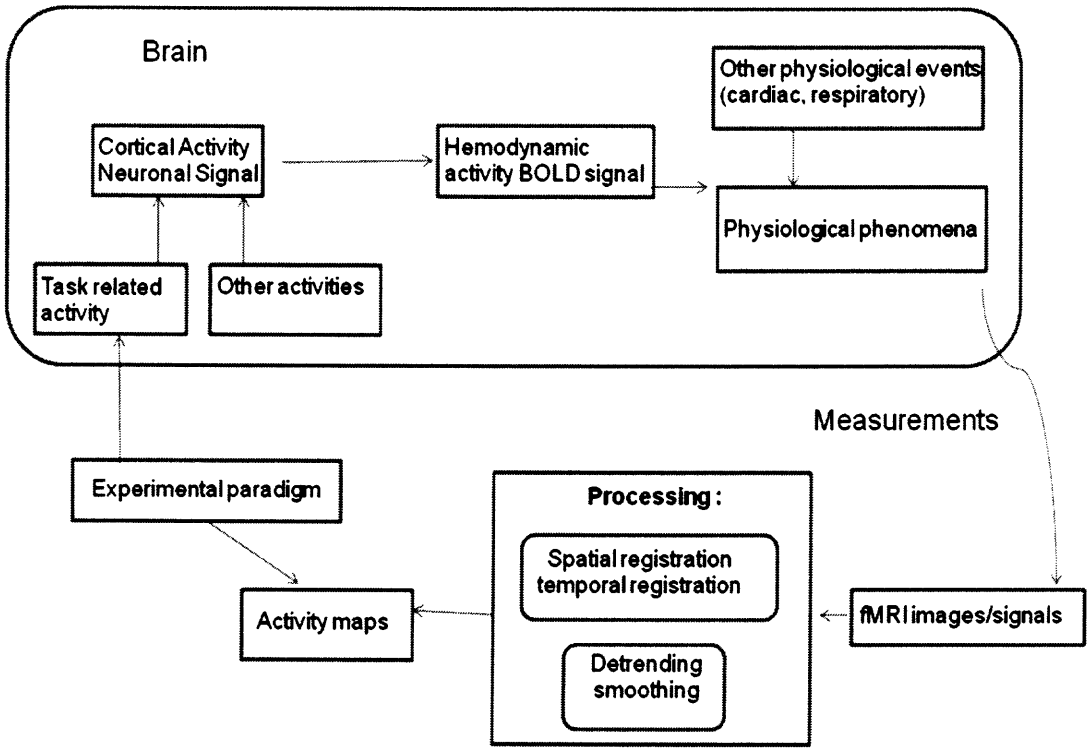

Figure 3.3 Schematic diagram of fMRI functioning and data processing.

3.6.1 Correlation

For the functional mapping of the brain a task is performed and fMRI data is acquired. The task performed by the subject corresponding to a stimulus/task. The assumption with most fMRI studies is that corresponding to the task/stimulus presentation, task induced signal changes in the brain changes in a similar fashion. Thus, correlation analysis assumes that the activation response is a scaled version of the stimulus response. Correlation of the reference stimuli/task is performed with for every voxel. Voxels showing a high correlation value corresponds to the region in the brain that was involve in the task performance.

3.6.2 Thresholding

In any data analysis procedure like a simple correlation a threshold value is used to classify the dataset into different regions. For correlation between the stimuli/task paradigms with the dataset a threshold value of about 0.4 is applied. Therefore, any region with a correlation coefficient value greater 0.4 was considered as active.

CHAPTER 4

METHOD

4.1 Subjects

Five healthy volunteers (4 males, 1 female) between 23-38 years of age, with no history of head trauma or neurological disease were scanned for this study. Written informed consent was obtained from all volunteers and all protocols approved by the local Institutional Review Board. Volunteers were recruited from an academic setting. Subjects were positioned supine on the scanner gantry with their head located at the coil midline. Foam padding was used to limit head motion, and subjects were provided with earplugs to attenuate scanner noise.

4.2 Experimental Paradigm

All five subjects performed two paradigms namely finger tapping and breath-holding. Each experiment started with a 25 second rest period followed by three repetitions of 75 second paradigm. The finger tapping and breath hold paradigm consisted of a block design of alternating periods of 25 seconds of respective task with periods of 50 seconds of rest. In two additional subjects, the duration of the breath holding was varied. Three scans were collected for which the period of breath holding consisted of 10, 20, and 25 seconds respectively. For the finger tapping task, subjects tapped their thumb with the other fingers in each hand in a self paced sequential manner for both hands. For the breath holding task, subjects performed an end-inspirational breath-holding. Stimulus instructions were given to the subjects through a microphone in the console room. The

finger tapping task was collected to test a different hypothesis and was not used for the study.

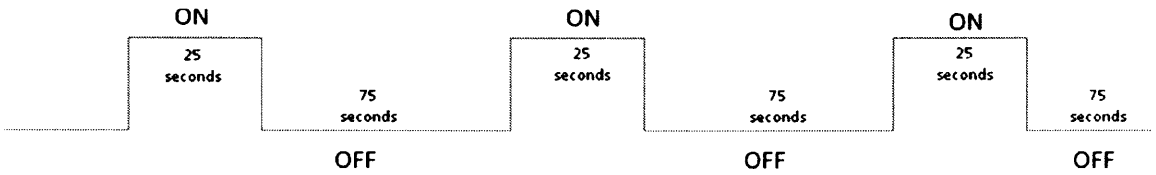

Figure 4.1 Task Paradigm: The subjects were asked to hold their breath during the ON period which was followed by a rest period, representing OFF in the diagram.

4.3 MRI Acquisition

All data were collected using a 3 Tesla Siemens Allegra MRI system (Siemens Medical System, Erlegen, Germany) specially equipped with a fixed asymmetric, balanced torque three-axis head gradient coil and a shielded end-capped quadrature transmit/receive RF coil. Subjects were positioned in a supine position on the gantry with head in a midline location in the coil. Foam padding and a pillow were used to minimize head motion.

The imaging procedure for each subject was as follows: Localizer images were obtained in the axial and sagittal planes using conventional gradient echo sequence (256 × 256, TR = 600 ms, TE = 10 ms, FOV = 20 cm). On the basis of these images, six axial slices passing through the sensorimotor cortex were selected for functional imaging. T1-weighted anatomical images were obtained across the motor cortex with a FOV of 200 mm^2, matrix size of 256X256, TR/TE = 380/14 msec, slice thickness = 7 mm, and a receiver bandwidth of 125 kHz. This resulted in a spatial resolution of 0.78 mm x 0.78 mm x 7mm. Gradient recalled echo–EPI images were obtained during finger tapping, and during breath-holding. The imaging parameters were: FOV of 20 x 20 cm2, matrix size of 64X64, TR/TE = 1000/30 msec, slice thickness of 7mm, flip angle of 80 degrees, and a

receiver bandwidth of 125 kHz. This resulted in a spatial resolution of 3.125 mm x 3.125 mm x 7 mm. 250 EPI images were obtained during both finger tapping, and during breath-holding.

4.4 Data Analysis

All fMRI data sets were preprocessed using AFNI [51]. The EPI images were corrected for motion using a rigid-body volume registration algorithm available in AFNI. All data sets that exhibited head motion were corrected prior to further analysis or discarded motion-induced artifact exceeded one voxel-shift. Analysis was done only on the voxels that represented the brain tissue. All the data sets were corrected for linear trends. Standard deviation (SD) of the voxel time course was used as a measure of signal variability. It was obtained on a voxel wise basis for the entire brain for each of the subjects for all paradigms. Maps of the SD were obtained during breath-holding.

4.4.1 Functional MRI Analyses

An idealized time-course representing an "ON/OFF" stimulus was used as a reference waveform for cross-correlation analysis to identify stimulus-locked responses [35]. Inherent to the cross-correlation technique is the assumption that neuronal activity and the fMRI signal vary synchronously with the stimulus paradigm – an assumption valid for the paradigm utilized in this study. Cross-correlation analyses identified voxels that had a shape similar to that of the reference waveform. If we represent the reference waveform (with a mean value of μ_r) by r_i and the voxel time-course (with a mean value

of μ_t) by t_i, where $i = 1,2,3.....N$ are the number of data points, the correlation-coefficient between the reference waveform r_i and the voxel time course t_i may be written as [35]:

$$cc = \frac{\sum_{i-1}^{N}(t_i - \mu_t)(r_i - \mu_r)}{\sqrt{\sum_{i=1}^{N}(t_i - \mu_t)^2 \sum_{i=1}^{N}(r_i - \mu_r)^2}} \qquad 12$$

For each scan, a histogram of the cross-correlation coefficients throughout the entire brain during rest was used to select a threshold coefficient for a valid response. Typically, only those correlation values were considered which were five times greater than the standard deviation of the resting state cross-correlation coefficient distribution. Using this criterion, a threshold correlation coefficient ≥ 0.4 guaranteed statistical significance ($p<0.001$) after including a correction for multiple comparisons.

4.4.2 Gamma-Variate Analyses

The breath holding data was fitted using the gamma-variate model on a voxel wise basis. The gamma-variate fit was optimized for each voxel time course. As a consequence, different gamma-variate fit parameters were obtained for each voxel in the brain. The onset time of the breath holding signal t_0 was determined from a gamma-variate fit to the image data on a voxel-wise basis (Fig. 3). The gamma-variate function is defined as:

$$S(t) = Q(t-t_0)^{re-(t-t_0)/b}) \qquad 13$$

Where $S(t)$ is the MR signal intensity, Q, r, b are fit constants, t is the time after injection, and t_0 is the appearance time of the tracer [28-29]. The t_0 value was determined for all voxels in the cortex, resulting in the generation of a t_0 map. In a similar fashion, Q, r, b, S_{max}, T_{max}, and S_{Area} maps were also generated for each of the subjects. The breath hold paradigm in this study was assumed to follow the tracer kinetics model. Recently, Cohen [52] has used a gamma-variate model to fit the fMRI impulse response function and correlated with the behavioral conditions to obtain a better prediction of the fMRI response. In their study, a very brief visual stimulus (for one second) was presented several times and fMRI response was averaged to obtain the impulse response function. Similarly, in this study the breath hold response was fitted to the gamma variate model, and several parameters including t_0, t etc were considered as the onset time of the fMRI response following the stimulus, while t represented the sampling rate. Non-linear regression was used to estimate the gamma-variate fit parameters using AFNI. Briefly it estimated the gamma-variate fit parameter using a predefined number (set as 1000 for this study) with signal and noise constraints. From the 1000 values of the parameters obtained, values from the five best fit parameters were selected.

To calculate the reliability of the estimation of the gamma-variate fit parameters, the breath holding data sets containing the three ON/OFF cycles were broken into three scans with one breath holding epoch in each of the data set. Identical gamma-variate analysis was performed for each of three data sets and the gamma-variate fit parameters were compared. A correlation analysis was performed between each of the gamma-variate fit parameter from the first data set with the corresponding parameter in the

second data sets. A bootstrap resampling method was used to test the reliability and confidence interval of the gamma-variate fit parameters. The parameters obtained from each of the three 'psuedo" runs were randomly selected to compute the correlation coefficient between the parameters. This process was repeated one thousand times.

4.4.3 ISODATA Clustering

A multi-parametric method, Iterative Self-Organizing Data Analysis Techniques (ISODATA) [22-23], was used to segment the tissue types into the gray matter, and white matter. As noted, the ISODATA technique is an unsupervised classification method that allows for categorization of an open-ended number of clusters, or tissue classes. The ability to adjust the number of potential dissociable clusters is the primary advantage of the ISODATA method because it requires no knowledge *a priori* of the exact number of clusters or their locations prior to segmentation. Similar multi-parametric methods have been used in stroke studies (both in animal models and human subjects) to demonstrate evolving heterogeneity within lesions [22-24]. In the ISODATA method, the minimum number of voxels for each cluster can be predetermined (i.e., cluster size is typically set at about 5-10 so that a single anomalous voxel cannot be its own tissue class). Each voxel in the image is then compared to the average value of the cluster to which it belongs. A mean cluster value is determined for all voxels from each of the clusters and the number of potential clusters, or tissue classes, is extracted from the data by the algorithm. This procedure is repeated for each tissue class until the Mean Squared Error (MSE) is minimized in each of the clusters (see Equation 3). The ISODATA algorithm thus allows for measurement of subtle, within-subject differences in voxel intensity,

which can then be used to identify the gray matter and white matter in an unbiased fashion. Moreover, the ISODATA method used here does not differentiate clusters through the use of an absolute hard threshold, which increases its flexibility and permits detection of subtle distinctions in tissue classes. ISODATA thus uses a soft threshold for clustering and a weighting strategy that incorporates information about the immediate environment of any cluster (e.g., cluster surrounded by similar or dissimilar tissue). Another reason for using ISODATA was that it could segment the gray matter or white matter using a single or multiple images.

The equation for calculating Mean Squared Error each of the clusters is:

$MSE = \Sigma [x-c(x)]^2 / (N-C)$	14

where x = a single voxel, c(x) is the mean value of cluster c, N is the number of voxels, and C is the number of clusters. For each of Gamma-variate fit parameters, ISODATA analysis was performed on each of the individual amps as well.

CHAPTER 5

RESULTS

Motion parameters were calculated for each subject during run. For each run, motion was estimated for each image with respect to a reference image (say image number 5) along all the six planes (x, y, z, xy, yz, xz). The calculated mean and standard deviation is shown in Table 1. It was seen that the motion was not significant during any of the runs in any of the subjects.

Table 5.1 Motion Parameters

Subject Number		X	Y	Z	XY	XZ	YZ
1		0.1237 ±0.1565	0.0145 ±0.1223	0.0193 ±0.0534	0.2709 ±0.2639	0.1412 ±0.1658	0.0555 ±0.1892
2		0.0538 ±0.0477	-0.0281 ±0.0115	0.0073 ±0.0126	0.1234 ±0.0594	0.0652 ±0.0807	0.0917 ±0.0355
3		-0.0088 ±0.0329	-0.0195 ±0.0219	-0.0571 ±0.0325	-0.0208 ±0.0330	-0.4870 ±0.1771	-0.0414 ±0.0326
4		-0.0695 ±0.0586	0.0122 ±0.0761	-0.0452 ±0.0444	-0.0052 ±0.0826	-0.1610 ±0.1290	-0.0154 ±0.1746
5	BH 10	-0.1567 ±0.0934	0.6038 ±0.3180	0.0535 ±0.0516	-0.3368 ±0.1869	-0.1611 ±0.0873	-0.0212 ±0.0162
	BH 20	-0.0250 ±0.0856	-.0996 ±0.1412	0.0038 ±0.0775	0.5098 ±0.1994	-0.1061 ±0.0758	-0.0250 ±0.0234
	BH 25	-0.2016 ±0.1110	-0.0104 ±0.1197	0.0551 ±0.0486	0.1652 ±0.1047	-0.2957 ±0.1055	0.0195 ±0.0214
6	BH 16	0.1364 ±0.0242	0.1234 ±0.0861	0.0132 ±0.0941	0.0917 ±0.1896	0.3011 ±0.0672	-0.1251 ±0.0953
	BH 20	-0.0269 ±0.0438	0.0833 ±0.0404	-0.0402 ±0.0522	0.0126 ±0.0580	-0.1550 ±0.0690	-0.1220 ±0.0871
	BH 30	-0.0197 ±0.0485	-0.0725 ±0.0767	-0.0423 ±0.0783	0.1458 ±0.1069	0.0575 ±0.0838	-0.0123 ±0.0444

Note: The motion parameters from all the four subjects during the breath hold scan is tabulated. Motion was estimated using a 3D volume registration method. Motion parameters were estimated along all the six parameters. The motion parameters were found not to be significant in any of the subjects during the breath hold scan. The mean and standard deviation of the motion parameters are listed for each of the subjects along all the six regions.

Significant amount of signal changes was observed in all the subjects during breath holding. After breath holding, increase in signal intensity was observed. The signal increased after an onset of about 15 seconds following breath holding. An idealized input waveform corresponding to the ON/OFF paradigm was shifted by 15 seconds (to account for the delay in response) and correlated with every voxel time series in the brain. All voxels with a correlation coefficient greater than 0.4 were considered active and classified as gray matter. The percent change in gray was significantly higher than in white matter region. The mean percent change in the gray matter from the first four subjects was 0.1864±0.2719, 0.1938±0.2756, 0.1987±0.2983, 0.3756±0.2675 respectively. However, there was a significant reduction in the mean percent change in white matter regions in all the four subjects compared to the gray matter regions. The mean percent change in the white matter for the four subjects were 0.0632±0.2287, 0.1412±0.2293, 0.0245±0.2391, 0.1491±0.2307 respectively. Figure 1A shows a representative voxel time courses from the gray matter regions. It can be seen that the signal changes corresponding to changes in the stimulus was observed in those voxels from the gray matter. Figure 1B shows corresponding maps of images that correlated significantly with the idealized reference Box-car function representing the breath holding timing.

A:

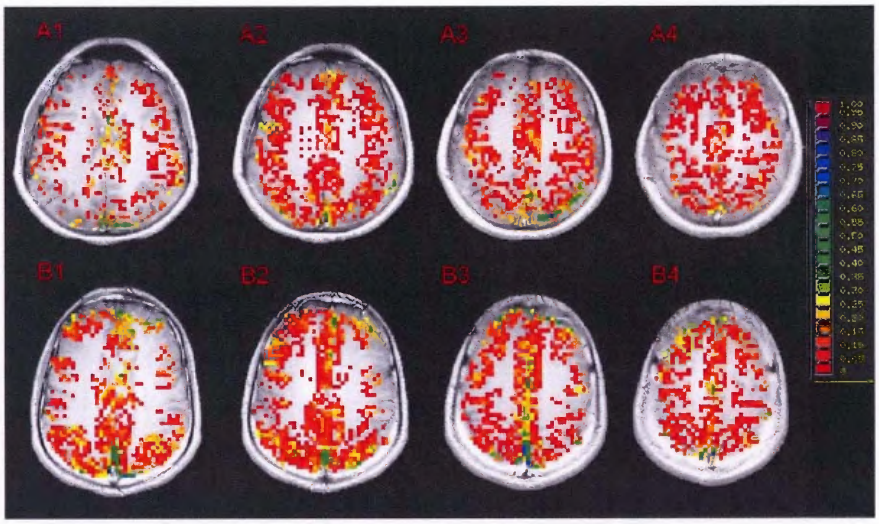

B:

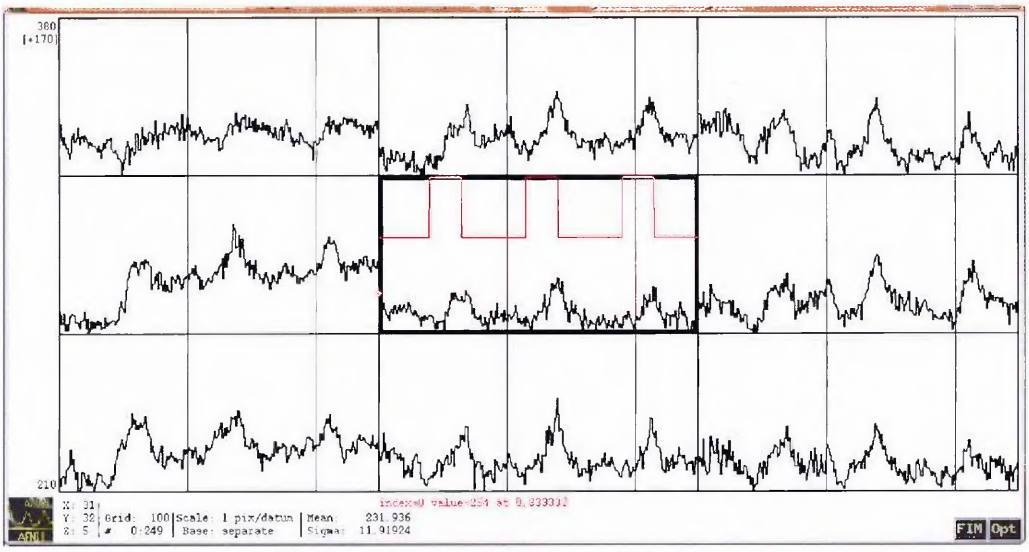

Figure 5.1 Breathe hold activation maps, ideal box paradigm with time series. A representative spatial map (A) showing voxels with significant changes during breath holding time series (B) is shown. During breath holding a significant change was observed in the gray matter region. Significantly less number of voxel from the white matter regions passed the threshold. The time series shows signal intensity changes in the gray matter during breath holding. It was typically seen that, the voxel time series from the gray matter changed by about 2.386 %. In the white matter though, a significantly lower amount of 0.945 %change was also observed.

The gamma-variate analysis was then used to fit every voxel time series in the brain. Each of the fit parameters was then estimated. Figure 2 shows representative voxel time series along with the gamma-variate fit parameters. Maps of the onset time (t_0), time to peak (T_{max}), maximum signal amplitude (S_{max}), and total area covered by the signal during the stimulus (S_{Area}), r, and b. Figure 3 shows spatial maps of each of the parameters from 2 representative subjects. A number of gamma-variate fit parameters including S_{max}, S_{Area}, t_0, T_{max}, r, and b showed good demarcation between the gray matter region,, the white matter regions. In a few cases regions from large vessels could be demarcated.

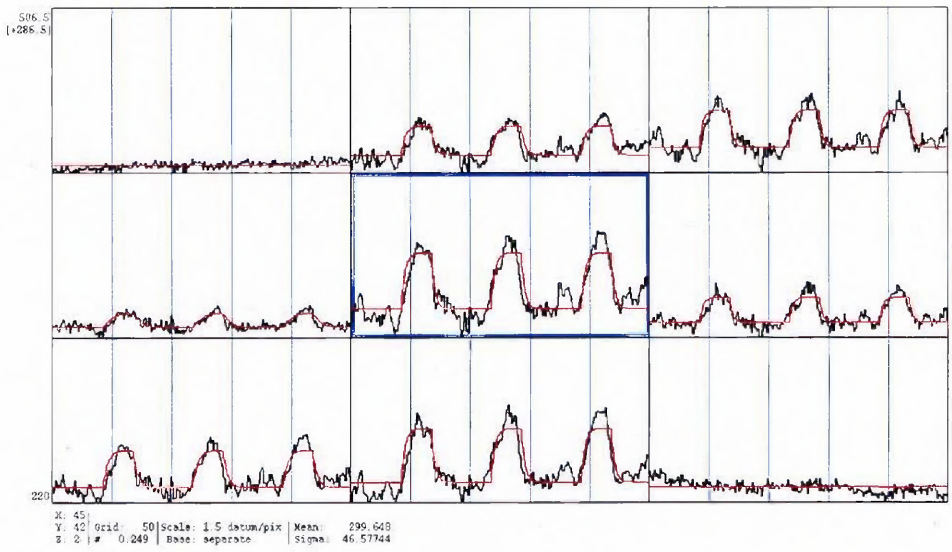

Figure 5.2 Gamma-variate fit. The gamma-variate fit parameters were calculated on a voxel-by-voxel basis for the entire brain. All the fit parameters including t0, a, b, r were then computed on a voxel by voxel basis. A 3x3 window of neighboring voxel time series along with the gamma-variate fit is shown. As can be seen the gamma-variate fit was able model the actual response from each of the epochs. Also, in the voxel time series where there was no signal change during breath hold task, the gamma-variate fit gave a good fit i.e. a straight line.

A:

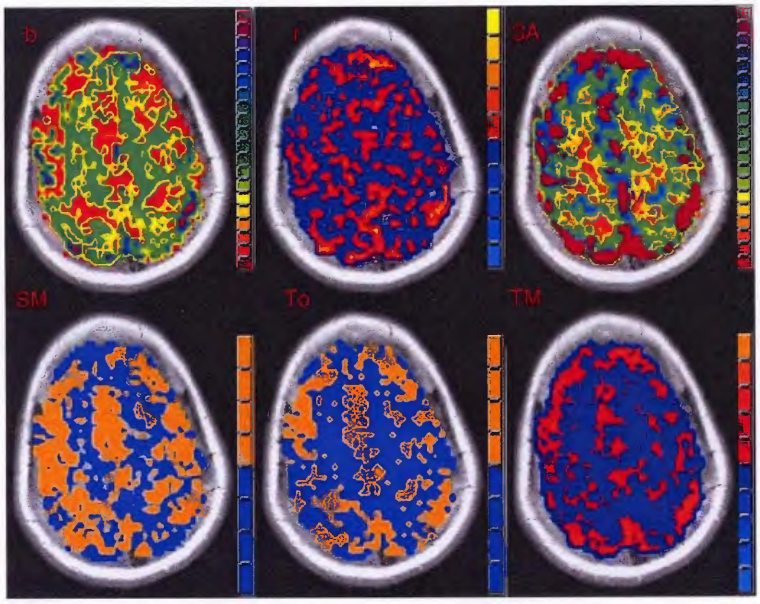

B:

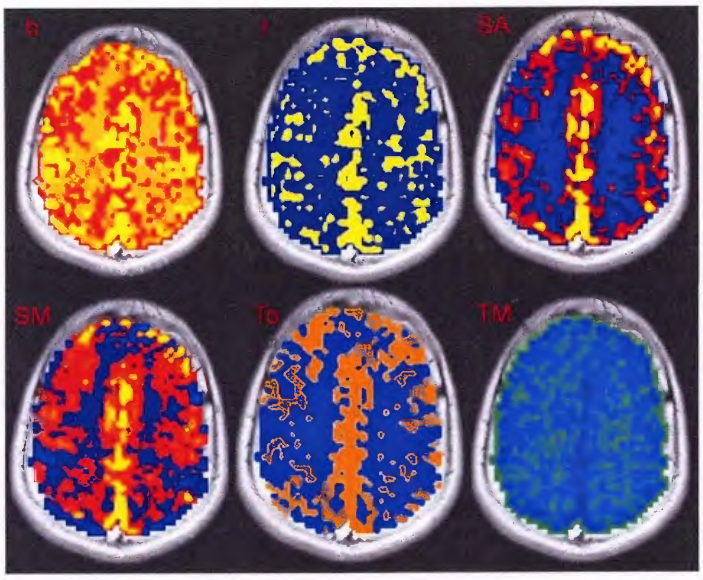

Figure 5.3 Maps of various gamma-variate fit parameters. The various parameters calculated through the gamma-variate fit including t_0, S_{max}, T_{max}, b, r, S_{Area}; were then used to show the activation maps. t_0, S_{Max} gave the better results compared to the other parameters. The parameters reflect the physiological characteristics of the underlying tissue. Representative images from two subjects are shown. It can be seen that the various parameters had differences between the gray matter and white matter regions. As can be seen the maps obtained from various parameters including t_0, S_{max}, S_{Area} resulted in good demarcation between the gray matter and the white matter regions.

Table 5.2 Gamma-variate parameters

Parameters / Subjects		T_0	Amp	R	b	Signal T_{max}	Signal S_{max}	Signal Area
1-sathe	Gray Matter	17.57 ±7.28	69.80 ±253.31	0.34 ±0.20	2.05 ±1.22	43.44 ±8.15	15.71 ±7.28	1084.73 ±713.3
	White Matter	11.82 ±6.28	22.29±2 57.3	0.24 ±0.19	1.53 ±0.19	39.46 ±6.67	5.73 ±3.41	396.12 ±218.0
2-chan	Gray Matter	11.30 ±6.27	80.14 ±238.18	0.29 ±0.21	3.15 ±0.97	26.89 ±5.68	13.76 ±7.87	102.43 ±114.8
	White Matter	8.32 ±5.37	68.32 ±213.64	0.21 ±0.19	1.79 ±1.10	25.88 ±4.50	6.28 ±5.69	54.73 ±64.43
3-biswal	Gray Matter	17.83 ±8.16	109.54 ±261.58	0.31 ±0.18	2.01 ±1.07	41.79 ±8.78	18.74 ±7.92	978.38 ±675.2
	White Matter	12.96 ±7.62	32.96 ±248.82	0.22 ±0.18	1.67 ±0.98	38.48 ±7.21	11.38 ±6.23	298.27 ±117.2
4-jaya	Gray Matter	16.58 ±8.79	97.42 ±260.71	0.28 ±0.19	1.98 ±1.13	42.23 ±8.19	12.19 ±6.51	382.76 ±452.9
	White Matter	7.91 ±7.18	15.31 ±223.56	0.20 ±0.15	1.36 ±0.85	39.16 ±5.74	7.37 ±8.12	198.32 ±178.1
5 BH 10	Gray Matter	14.35 ±4.72	594.53 ±430.55	0.492 ±0.17	1.98 ±1.34	42.75 ±8.02	9.73 ±4.61	178.21 ±132.8
	White Matter	12.27 ±3.73	331.73 ±349.12	0.35 ±0.15	1.32 ±0.86	38.18 ±2.46	6.36 ±3.61	70.27 ±39.12
5 BH 20	Gray Matter	13.08 ±5.04	598.13 ±342.83	0.47 ±0.19	2.01 ±1.22	45.64 ±6.31	10.72 ±3.87	198.54 ±143.7
	White Matter	11.62± 3.675	287.18± 362.21	0.33 ±0.14	1.41 ±0.97	41.62 ±2.71	7.21 ±2.91	67.27 ±48.72
5 BH 25	Gray Matter	12.02 ±3.92	613.26 ±263.65	0.52 ±0.17	2.13 ±1.13	47.51 ±5.09	9.67 ±3.82	187.28 ±128.8
	White Matter	11.63 ±3.92	387.65 ±283.83	0.31 ±0.13	1.34 ±0.96	41.76 ±2.76	5.65 ±3.10	73.29 ±36.28
6 BH 10	Gray Matter	13.77 ±3.28	671 ±365	0.40 ±0.27	2.31 ±1.27	39.72 ±7.36	11.83 ±5.67	74.26 ±39.27
	White Matter	11.25 ±4.08	452 ±198	0.31 ±0.22	1.46 ±1.01	34.14 ±5.65	7.78 ±3.65	35.21 ±27.54
6 BH 20	Gray Matter	13.58 ±3.86	597 ±237	0.44 ±0.28	2.10 ±1.16	43.87 ±6.63	12.17 ±5.28	148.63 ±79.26
	White Matter	11.76 ±4.18	287 ±182	0.39 ±0.19	1.56 ±1.23	38.72 ±5.36	8.19 ±4.98	69.46 ±56.52
6 BH 30	Gray Matter	12.79 ±3.92	548 ±199	0.42 ±0.23	2.18 ±1.13	52.29 ±6.78	11.87 ±6.21	163.17 ±86.17
	White Matter	10.59 ±4.09	392 ±178	0.37 ±0.18	1.63 ±1.28	40.18 ±5.87	7.36 ±3.98	89.53 ±54.92

Note: Spatial overlap was computed between the manually traced white matter regions with the white matter computed using the breath holding based segmentation method. In a similar fashion, the spatial overlap for the gray matter region was also calculated between the manually traced and the breath holding based segmentation based method.

Table 2 shows the mean of the various gamma-variate fit parameters including t_0, amp, r, b, etc in the gray matter and white matter regions for each of the subjects. Statistical comparisons were made between the gray matter, white matter region, and large vessels. Significant difference was observed between the gray matter, white matter, and large vessels values for various parameters. Signal area (S_{Area}) and t_0 showed the greatest difference between the two regions. The ratio between the gray matter and white matter for signal areas varied between 3.11 and 2.09 with a mean value of 2.56.

For the two subjects, from which three different breath hold periods was used, no significant differences between the gamma variate fit parameters were observed. The to fit parameters during the three breath holding period for the two subjects were 14.35, 13.08, 12.02, and 13.77, 13.58, and 12.79 respectively. Similarly, the variations between other fit parameters were also minimal. Table 2 shows the fit parameters for the two subjects.

5.1 Reliability of Gamma-Variate parameters

To calculate the reliability of the estimation of the gamma-variate fit parameters, data sets containing the three ON/OFF cycles were broken into three scans with one breath holding epoch in each of the data set. Identical analysis was performed for each of the three data sets and the gamma-variate fit parameters compared. A correlation analysis was performed between each of the gamma-variate fit parameters from the first data set with the corresponding parameter in the second data sets. The correlation coefficient for a representative subject (#2) was found to be 0.8804±0.0110. Figure 4 shows a representative scatter plot between the signal areas that was computed for the first run

compared with the signal area from the corresponding voxel in the second run. A significant overlap between the two with R^2= 0.7533 was found.

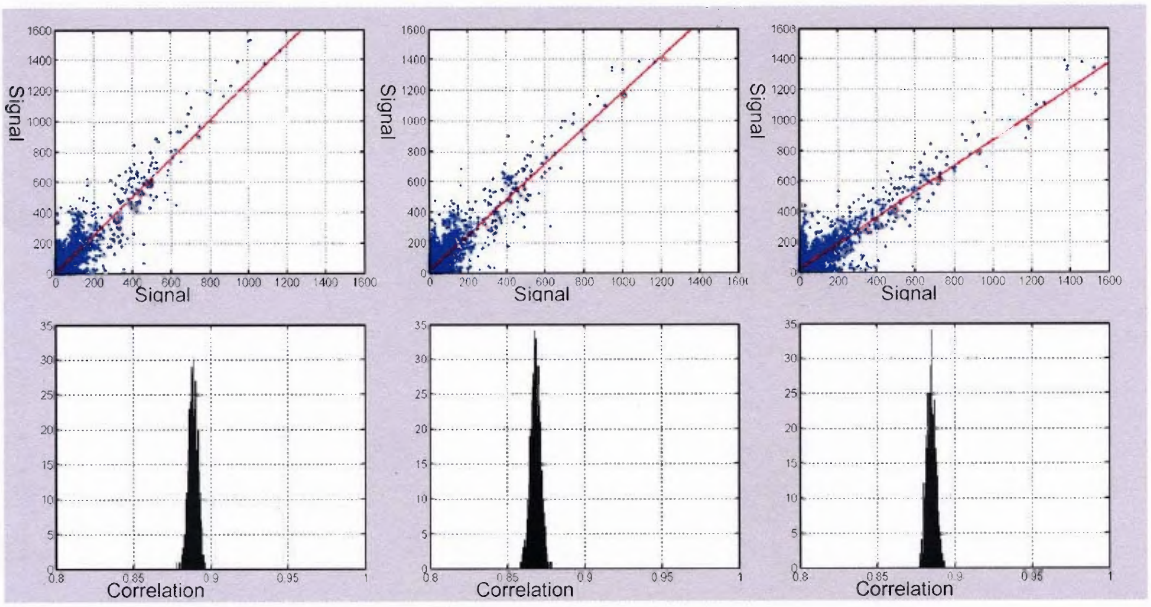

Figure 5.4 Test-Retest Reliability of Gamma-variate fit Parameters. The scan containing three breath hold paradigms was broken into three "pseudo" runs, each run consisting of one breath holding task. The gamma-variate fit parameters were calculated for each of the runs on a voxel wise basis. This figure shows the signal area computed for the first run compared with the signal area from the corresponding voxel in the second run. A significant overlap (R2=0.7533) was observed between the two. Comparison between the first and third, and second and third also showed significant correlations (mean value and standard deviation of 0.8804±0.0110).

Images representing the gamma-variate fit parameters were then clustered using ISODATA. For this study six clusters were used to take into account gray matter, and white matter and other noise sources. In every subject, two distinct classes of clusters representing the gray matter, and the white matter were observed. The other clusters in some subjects represented edges of the brain, large vessels, and other noise sources. Figure 5 shows comparison of gray matter, white matter segmentation using high

resolution image with segmentation obtained using gamma-variate fit parameters obtained during breath holding.

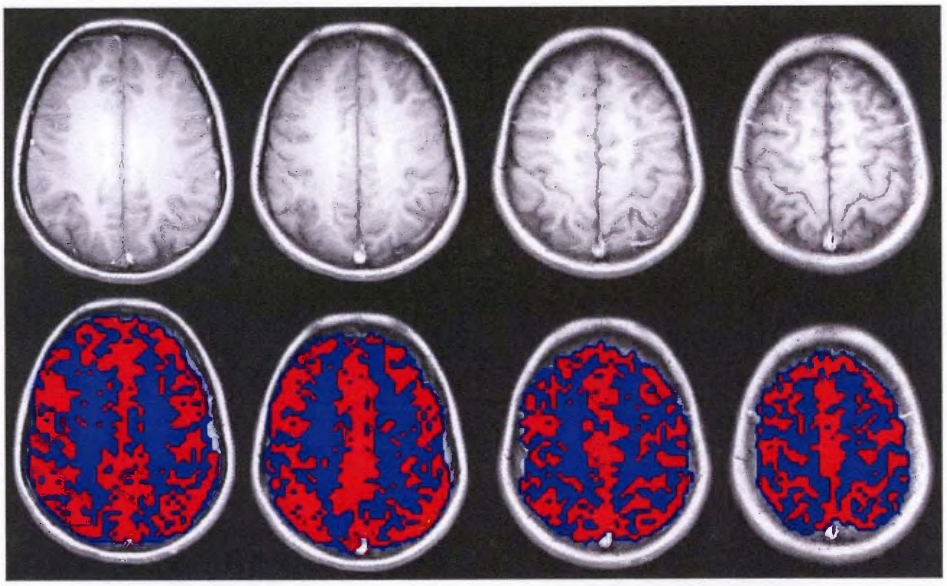

Figure 5.5 Anatomical clustering: As a validation, high resolution anatomical images were processed in an identical fashion as that obtained from parameters obtained from data during the breath holding using the gamma-variate fit. In addition to using the same ISODATA algorithm, the region of interest, the numbers of clusters were also kept the same. High resolution images (A) along with the clustered image using (B) the gamma-variate fit parameters are shown.

The high resolution anatomical data obtained from each of the subjects were also clustered using ISODATA. Identical clustering parameters as used by the gamma-variate fit parameter data was also used for this study. The same parameters were used to arrive at the same number tissue types. Using ISODATA, in every subject, unique clusters corresponding to the gray matter and the white matter were seen. A significant correlation of 0.88 was observed between the region identified by the ISODATA as gray matter and manually traced gray matter. Similar results were also observed in the white matter also.

CHAPTER 6

DISCUSSION AND FUTURE WORK

This study demonstrates the use of breath hold as a novel method for segmenting tissue types. Using data sets obtained during breath holding in each of the subject, segmentation between gray matter, and white matter was achieved. A substantial overlap with the gray matter and white matter from high resolution MRI images with the corresponding voxels determined using breath holding data was found. Further, the breath holding data could identify large vessels present in the time series data sets.

The use of breath hold as an alternative to traditional contrast agent studies provides a numerous advantages. For example, using Gadolinium (Gd) only a certain volume of contrast agent can be given to a subject. If the images obtained during this time were contaminated by imaging artifacts or patient motion, the data set can not be used for the gamma-variate fit, since it would lead to errors in the estimates. In contrast, for breath holding studies, several scans can be obtained without having to worry about the dosage level, since an additional breath holding scan can easily be obtained. The effects of recirculation in breath holding will also be minimal compared to that obtained using contrast agent. Further, recent studies have shown that contrast agents may have deleterious effects in certain patient populations, especially patients with kidney diseases. With the wide spread use of fMRI, the origins of the signals and ways to quantify the signal is becoming important. A number of groups including [40-42] have demonstrated using breath holding that the task induced fMRI signal can be normalized to account for regional differences in cerebro-vascular reactivity. As a result, there are several groups that are currently performing breath holding studies in addition to functional and

anatomical scanning. Therefore, using an experimental breath hold paradigm in addition to calibrating the fMRI signal, tissue segmentation can be performed to differentiate between tissue types. Thus, using a simple procedure like breath holding tissue segmentation especially between gray matter and white matter can be performed in addition to calibrating the fMRI response.

The segmentation obtained in this study was generated using various physiological parameters including t_0, T_{max}, S_{max}, S_{Area} etc. The various physiological factors were obtained using an fMRI scan. This study suggests that each of those parameters can be used to segment the fMRI data into gray matter, and white matter regions. In a few subjects with slices containing large vessels, differences in the gamma variate fit parameters (compared with gray matter and white matter) was observed. In this study, the t_0, and S_{Area} parameters from each data set had the greatest demarcation between the gray matter and white matter regions. We are currently investigating the use of parameters that can be used to optimize the tissue segmentation. It is quite possible, that for clinical patients, some of the above parameters can be used to differentiate between healthy and diseased tissue types.

Although a good overlap between the gray matter and white matter was obtained from the fMRI response during the BOLD imaging, a direct comparison between the gray matter and the white matter using DSC was not done in this study. A direct comparison between the two methods will provide further validation and differences between the two methods and the sensitivity between the tissue types. We are currently evaluating a direct comparison between DSC using Gd and the breath holding method presented here.

The segmentation method presented here may prove useful in a number of clinical environments. For example, tumor detection and gradation may be obtained using breath holding. Similarly in patients with stroke, lesion detection may be accomplished using breath hold based segmentation. For clinical patients, where physiological parameters including cerebral blood flow and cerebral blood volume have been compromised, an investigation of these physiological parameters may provide clinically relevant information. In addition to using a combination of these parameters, specific parameters can be used to differentiate between healthy and diseased tissue types. However, if the diseased region is from an area where the underlying neurovasculature has not been affected it is likely that breath holding will not be able to differentiate the diseased region from the healthy tissues.

With the growing recognition of fMRI, a large number of studies are currently being performed in patient populations. For example, in presurgical mapping, in addition to obtaining the functionally relevant regions surrounding the tumour, the underlying characteristics of the tumor are also collected with high resolution anatomical imaging. High resolution anatomical imaging on an average take several minutes to complete, and more than one type of sequences are typically collected. With fMRI, from a single breath hold scan which would take about 2 minutes, various gamma variate fit parameters could be obtained to segment the images. Further, with the increasing use of breath holding and other vasodilation methods including hypercapnia to normalize the fMRI task activation signal, the data set collected during the breath holding scan may further be utilized for tissue segmentation.

All the data obtained for this study was obtained used gradient echo EPI images. The gradient echo EPI images are known to be sensitive to medium and large vasculature, and are not very sensitive to small size vasculature [53]. As a result, the signal obtained is selectively modulated based on the underlying vasculature. As a consequence, high signal to noise was obtained from regions with gray matter and large vessels, thus making signal detection and differentiation possible compared to the white matter regions. Alternative pulse sequences including spin echo EPI method which is more sensitive to small and medium size vessels could be used for the breath hold, and the gamma variate fit parameters compared between the gradient echo and spin echo EPI images.

For this study, three different breath holding durations of 10, 20, and 25 seconds were used in two subjects, to determine the variability of the gamma variate fit parameters and the corresponding segmentation of gray matter and white matter. It was found that the 20 second breath holding gave the best parameters. It is possible that this is because, while 10 seconds was too short for the breath hold induced signal response to reach peak amplitude and good signal to noise ratio, resulting in suboptimal estimates of the gamma variate fit parameters. Because not statistical differences between the gamma variate fit parameters was observed between the 20 second and 25 second breath holding, 20 seconds could be used in future studies since, it would cause less discomfort (and probably less head motion) compared to longer breath holds.

Various physiological estimates including CBF, CBV, and MTT have not been measured and validated for this study. We are currently in the process of conducting studies where both the Gd and breath holding data is obtained in the same subject under identical

imaging parameter during same session. Such a study could then be used to validate the physiological parameters obtained during the paradigms. Nonetheless, the current study demonstrates the use of breath holding as a way of differentiating and segmenting between gray matter, white matter, and large vessels.

Although Gamma variate fit parameters were used for this study, it is quite likely that other analysis methods could be used to obtain parameters that could be used to segment tissue types. For example, standard deviation of the time series data could be used to obtain some level of differentiation albeit not as robust as the gamma variate fit parameters. For example, Kao et al, (34) have recently used ICA in conjunction with Bayesian estimation to differentiate between tissue types from data obtained using the contrast injection. Such methods could be modified to be used for the existing study. Other curve fit strategies including methods developed for pharmacokinetic models could probably give a better fit to the fMRI hemodynamic response. We are currently exploring the use of various data driven as well model driven method to obtain robust tissue differentiation types.

To segment the gray matter and the white matter, the gamma-variate parameters were segmented using Euclidian distance. The clustering algorithm used k-means algorithm to identify and segment the regions into a number of different types. The k-means algorithm uses a number of assumptions including the Gaussian nature of noise, etc. If these parameters were violated, the segmentation may not be optimal. While Euclidean distance was computed for this study, other metrics including independent or correlated parameters are currently being investigated.

One limitation of using breath holding is that subject compliance is required. It is possible that in several clinical or special patient populations, breath holding is either very difficult or not possible. For example, in aging or pediatrics population breath holding is very difficult to achieve, and compliance to it also becomes an issue without external monitoring. Further, in patient populations in intensive care, breath holding will be difficult. However, as an alternative to breathe holding, other hypercapnic stimulation methods including, breathing of 2% - 5% CO2 gas mixture could be used. Further, with some patient training such studies may become easier to perform.

REFERENCES

1. Clarke LP, Velthuizen RP, Camacho MA, Heine JJ, Vaidyanathan M, Hall LO, Thatcher RW, Silbiger ML. MRI segmentation: methods and applications. Magn Reson Imaging. 1995;13:343-368.

2. Wallace CJ, Seland TP, Fong TC. Multiple sclerosis. The impact of MR imaging. AJR. 1992;158:849-857.

3. Kapouleas I. Automatic detection of white matter lesions in magnetic resonance brain images. Comput. Meth. Progr. Biomed. 1990;32:17-35.

4. Liang Z. Tissue classification and segmentation of MR images. IEEE Eng. Med. Biol. 1993;12:81-85.

5. Bandettini PA, Wong EC, Hinks RS, Tikofsky RS, Hyde JS. Time course EPI of human brain function during task activation. Magn Reson Med. 1992;25:390-397.

6. Belliveau JW, Kennedy DN Jr, McKinstry RC, Buchbinder BR, Weisskoff RM, Cohen MS, Vevea JM, Brady TJ, Rosen BR. Functional mapping of the human visual cortex by magnetic resonance imaging. Science. 1991;254:716-719.

7. Kwong KK, Belliveau JW, Chesler DA, Goldberg IE, Weiskoff RM, Poncelet BP, Kennedy DN, Hoppel BE, Cohen MS, Turner R, Rosen B, Brady TJ. Dynamic magnetic resonance imaging of human brain activity during primary sensory stimulation. Proc Natl Acad Sci USA. 1992;89:5675-5679.

8. Ogawa S, Tank DW, Menon R, Ellermann JM, Kim SG, Merkle H, Ugurbil K. Intrinsic signal changes accompanying sensory stimulation: functional brain mapping with magnetic resonance imaging. Proc Natl Acad Sci U S A. 1992;89:5951-5955.

9. DeYoe EA, Bandettini P, Neitz J, Miller D, Winans P. Functional magnetic resonance imaging (FMRI) of the human brain. J. Neurosci Methods. 1994;54:171-187.

10. Just M, Thelen M. Tissue characterization with T1, T2, and proton density values: Results in 160 patients with brain tumors. Radiology 1988;169:779-785.

11. Higer PH and Gernot B. Tissue Characterization in MR Imaging: Clinical and Technical Approaches. New York: Springer; 1990.

12. Suzuki H, Toriwaki J. Automatic segmentation of head MRI images by knowledge guided thresholding. Comput Med Imaging Graph. 1991;15:233-240.

13. Filippi M, Rovaris M, Campi A, Pereira C, Comi G. Semi-automated thresholding technique for measuring lesion volumes in multiple sclerosis: effects of the

change of the threshold on the computed lesion loads. Acta Neurol Scand. 1996;93:30-34.

14. Huh S, Ketter TA, Sohn KH, Lee C. Automated cerebrum segmentation from three-dimensional sagittal brain MR images. Comput Biol Med. 2002;32:311-328.

15. Tang H, Wu EX, Ma QY, Gallagher D, Perera GM, Zhuang T. MRI brain image segmentation by multi-resolution edge detection and region selection. Comput Med Imaging Graph. 2000;24:349-357.

16. Schnack HG, Hulshoff Pol HE, Baare WF, Staal WG, Viergever MA, Kahn RS. Automated separation of gray and white matter from MR images of the human brain. Neuroimage. 2001;13:230-237.

17. Webb J, Guimond A, Eldridge P, Chadwick D, Meunier J, Thirion JP, Roberts N. Automatic detection of hippocampal atrophy on magnetic resonance images. Magn Reson Imaging. 1999;17:1149-1161.

18. Hu S, Collins DL. Joint level-set shape modeling and appearance modeling for brain structure segmentation. Neuroimage. 2007;36:672-683.

19. Soltanian-Zadeh H, Windham JP, Peck DJ, Mikkelsen T. Brain tumor segmentation and characterization by pattern analysis of multispectral NMR images. NMR Biomed. 1998;11:201-208.

20. Soltanian-Zadeh H, Peck DJ. Feature space analysis: effects of MRI protocols. Med Phys. 2001;28:2344-51.

21. Soltanian-Zadeh H, Windham JP. Mathematical basis of eigenimage filtering. Magn Reson Med. 1994;31:465-467.

22. Jacobs MA, Zhang ZG, Knight RA, Soltanian-Zadeh H, Goussev AV, Peck DJ, Chopp M. A model for multiparametric MRI tissue characterization in experimental cerebral ischemia with histological validation in rat: part 1. Stroke. 2001;32:943-949.

23. Jacobs MA, Mitsias P, Soltanian-Zadeh H, Santhakumar S, Ghanei A, Hammond R, Peck DJ, Chopp M, Patel S. Multiparametric MRI tissue characterization in clinical stroke with correlation to clinical outcome: part 2. Stroke. 2001;32:950-957.

24. Mitsias PD, Jacobs MA, Hammoud R, Pasnoor M, Santhakumar S, Papamitsakis NI, Soltanian-Zadeh H, Lu M, Chopp M, Patel SC. Multiparametric MRI ISODATA ischemic lesion analysis: correlation with the clinical neurological deficit and single-parameter MRI techniques. Stroke. 2002;33:2839-2844.

25. Rosen BR, Belliveau JW, Vevea JM, Brady TJ. Perfusion imaging with NMR contrast agent. Magn Reson Med. 1990;14:249-265.

26. Villringer A, Rosen BR, Belliveau JW, Ackerman JL, Lauffer RB, Buxton RB, Chao YS, Wedeen VJ, Brady TJ. Dynamic imaging with lanthanide chelates in normal brain: contrast due to magnetic-susceptibility effects. Magn Reson Med. 1988;6:164–174.

27. Gillis P, Koenig SH. Transverse relaxation of solvent protons induced by magnetized spheres: application to ferritin, erythrocytes, and magnetite. Magn Reson Med. 1987;5:323–345.

28. Zierler KL. Equations for Measuring Blood Flow by External Monitoring of Radioisotopes. Circ. Res. 1965;16:309-321.

29. Zierler KL. Tracer-dilution techniques in the study of microvascular behavior. Fed Proc. 1965;24:1085-1091.

30. Østergaard L, Weisskoff RM, Chesler DA, Gyldensted C, Rosen BR. High resolution measurement of cerebral blood flow using intravascular tracer bolus passages. I. Mathematical approach and statistical analysis. Magn Reson Med. 1996;36:715–725.

31. Østergaard L, Sorensen AG, Kwong KK, Weisskoff RM, Gyldensted C, Rosen BR. High resolution measurement of cerebral blood flow using intravascular tracer bolus passages. II. Experimental comparison and preliminary results. Magn Reson Med. 1996;36:726–736.

32. Law M, Young R, Babb J, Pollack E, Johnson G. Histogram analysis versus region of interest analysis of dynamic susceptibility contrast perfusion MR imaging data in the grading of cerebral gliomas. AJNR Am J Neuroradiol. 2007;28:761-766.

33. Perkio J, Soinne L, Ostergaard L, Helenius J, Kangasmaki A, Martinkauppi S, Salonen O, Savolainen S, Kaste M, Tatlisumak T, Aronen HJ. Abnormal intravoxel cerebral blood flow heterogeneity in human ischemic stroke determined by dynamic susceptibility contrast magnetic resonance imaging. Stroke. 2005;36:44-49.

34. Kao YH, Guo WY, Wu YT, Liu KC, Chai WY, Lin CY, Hwang YS, Jy-Kang Liou A, Wu HM, Cheng HC, Yeh TC, Hsieh JC, Mu Huo Teng M. Hemodynamic segmentation of MR brain perfusion images using independent component analysis, thresholding, and Bayesian estimation. Magn Reson Med. 2003;49:885-894.

35. Bandettini PA, Jesmanowicz A, Wong EC, Hyde JS. Processing strategies for time-course data sets in functional MRI of the human brain. Magn Reson Med. 1993;30:161-173.

36. Ward BD, Mazaheri Y. State-space estimation of the input stimulus function using the Kalman filter: a communication system model for fMRI experiments. J Neurosci Methods. 2006;158:271-278.

37. Boynton GM, Engel SA, Glover GH, Heeger DJ. Linear systems analysis of functional magnetic resonance imaging in human V1. J Neurosci. 1996;16:4207-4021.

38. Kastrup A, Kruger G, Glover GH, Moseley ME. Assessment of cerebral oxidative metabolism with breath-holding and fMRI. Mag Reson Med. 1999;42:608-611.

39. Kastrup A, Kruger G, Neumann-Haefelin T, Glover GH, Moseley ME. Changes of cerebral blood flow, oxygenation, and oxidative metabolism during graded motor activation. Neuroimage. 2002;15:74-82.

40. Li TQ, Kastrup A, Takahashi AM, Mosley ME. Functional MRI of human brain during breath-holding by BOLD and FAIR techniques. Neuroimage. 1999;9:243-249.

41. Thomason ME, Burrows BE, Gabrieli JD, Glover GH. Breath holding reveals differences in fMRI BOLD signal in children and adults. Neuroimage. 2005;25:824-837.

42. Kannurpatti SS, Biswal BB, Hudetz AG. Differential fMRI-BOLD signal response to apnea in humans and anesthetized rats. Magn Reson Med. 2002;47:864-870.

43. Kastrup A, Kruger G, Glover GH, Neumann-Haefelin T, Moseley ME. Regional variability of cerebral blood oxygenation response to hypercapnia. Neuroimage. 1999;10:675-681.

44. Bandettini PA, Wong EC. A hypercapnia-based normalization method for improved spatial localization of human brain activation with fMRI. NMR Biomed. 1997;10:197-203.

45. Brown GG, Eyler Zorrilla LT, Georgy B, Kindermann SS, Wong EC, Buxton RB. BOLD and perfusion response to finger-thumb apposition after acetazolamide administration: differential relationship to global perfusion. J Cereb Blood Flow Metab. 2003;23:829-837.

46. Ito H, Ibaraki M, Kanno I, Fukuda H, Miura S. Changes in cerebral blood flow and cerebral oxygen metabolism during neural activation measured by positron emission tomography: comparison with blood oxygenation level-dependent contrast measured by functional magnetic resonance imaging. J Cereb Blood Flow Metab. 2005;25:371-377.

47. Uludag K, Dubowitz DJ, Yoder EJ, Restom K, Liu TT, Buxton RB. Coupling of cerebral blood flow and oxygen consumption during physiological activation and deactivation measured with fMRI. Neuroimage. 2004;23:148-155.

48. An H, Lin W, Celik A, Lee YZ. Quantitative measurements of cerebral metabolic rate of oxygen utilization using MRI: a volunteer study. NMR Biomed. 2001;14:441-447.

49. Biswal BB, Kannurpatti SS, Rypma B. Hemodynamic scaling of fMRI-BOLD signal: validation of low-frequency spectral amplitude as a scalability factor. Magn Reson Imaging. 2007 (In Press).

50. Zierler K. Indicator dilution methods for measuring blood flow, volume, and other properties of biological systems: a brief history and memoir. Ann Biomed Eng. 2000;28:836-848.

51. Cox RW, Hyde JS. Software tools for analysis and visualization of fMRI data. NMR Biomed. 1997;10:171-178.

52. Cohen MS. Parametric analysis of fMRI data using linear systems methods. Neuroimage. 1997;6:93-103.

53. Bandettini PA, Wong EC, Jesmanowicz A, Hinks RS, and Hyde JS. Spin-echo and gradient-echo EPI of human brain activation using BOLD contrast: a comparative study at 1.5 T. NMR Biomed. 1994;7:12-20.

54. Bomans M., Hohne K.H., Tiede U., Riemer M. 3-D segmentation of MR images of the head for 3-D display. IEEE Trans. Med. Imaging. 1990;9:177-183;

55. Canny J. A computational approach to edge detection. IEEE Trans. Patt. Anal. Machine Intell. 1986;8:679-698.

56. Li H., Manjunath B.S., Mitra S.K. A contour-based approach to multisensor image registration. IEEE Transactions, Image Processing. 1995;4:320-334.